Imprint of transition metal d-orbitals on graphene Dirac cone (Supplemental material)

Qin Zhou, Sinisa Coh, Marvin L. Cohen, Steven G. Louie, and A. Zettl

Department of Physics, University of California at Berkeley and Materials Sciences Division, Lawrence Berkeley National Laboratory, Berkeley, California 94720, USA

1. CVD growth of graphene on platinum

Graphene growth has been carefully carried out to produce high quality samples. The original recipe we used was identical to Ref. [1], annealing platinum foil in 1 atm hydrogen environment for 10 minutes at 1040 °C followed by growth using 700 sccm of hydrogen and 5 sccm of methane at the same temperature. We noticed that the growth carried out this way produces graphene with black dots (Figure S1). The Raman signal of this type of sample appears to be inhomogeneous without the local consistency mentioned in the main text. The black dots are characterized in a very recent study [2] to be randomly oriented nanocrystalline graphene puddles residing between the graphene and platinum.

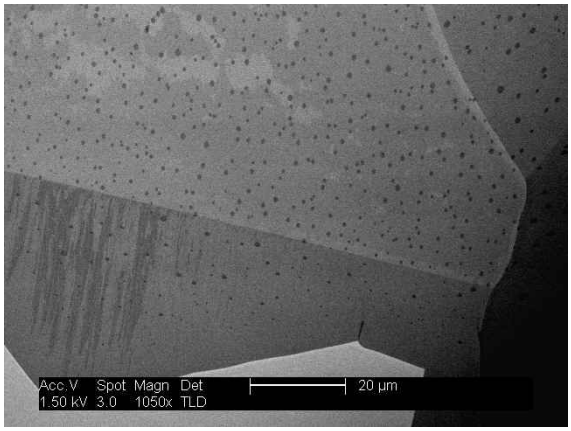

Figure S1. graphene grown at 1040 °C without pre-oxygen cleaning and long-time hydrogen anneal.

With the same growth condition, if the platinum foil is first heated to 1100 °C in air for 30 minutes and annealed in hydrogen for 1 hour before the growth, the black dot density can be noticeably reduced (Figure S2).

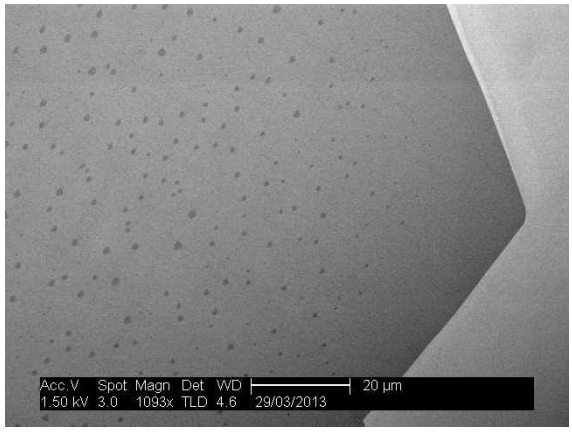

Figure S2. The pre-treatment of oxygen and hydrogen annealing of platinum foil is an essential step to reduce the black dot density.

We found the black dot can be further reduced to negligible level if we lower the growth temperature (Figure S3). In this approach, the foil is pre-treated with sequential oxygen and hydrogen annealing at 1100 °C as before, and the growth is carried out at 950 °C. The gas flow rate is 700 sccm for hydrogen, and 10 sccm for methane, respectively. The methane flow rate is increased because at 950 °C 5 sccm methane flow does not initiate graphene growth. At this growth temperature, the acquired graphene can still be of large grain size of approximately a hundred microns and of high quality as verified by Raman spectroscopy on transferred graphene on SiO_2/Si substrate. Most of our measurements are done on this type of samples. We note that further increasing the methane concentration will accelerate the graphene growth but decrease the graphene crystal size and quality. We also note that graphene grown on copper at this temperature usually have small grain size and large Raman D peak, indicating the presence of defects. This is probably due to much higher catalytical activity of platinum [1].

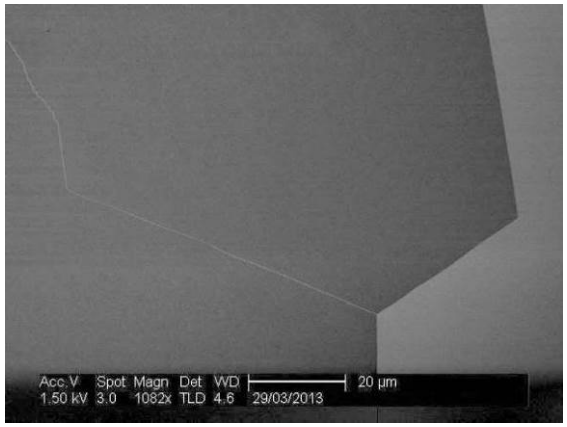

Figure S3. Graphene grown on Pt with optimized growth condition shows little black dots.

The detailed growth process is described here. Platinum (111) single crystal or 0.1 mm-thick polycrystalline platinum foil is cleaned and by acetone, IPA, DI water and followed by oxygen plasma, and is loaded into a 1-inch-diameter quartz tube in a CVD furnace. The tube is heated to 1100 °C in air for 30 minutes, and is then pumped down to 30 mTorr vacuum pressure. The pumping process takes approximately 5 minutes. Hydrogen is introduced at 20 sccm, and the tube pressure is 180 mTorr. After flushed with hydrogen for 10 minutes, the pump is turned off and the hydrogen is turned to the maximum

flow to bring the pressure to 1 atm. After the pressure reached 1 atm, the hydrogen flow is stabilized at 700 sccm. The temperature of the furnace is kept at 1100 °C and the annealing process last 1 hour. The temperature is then turned down to 950 °C. Once the temperature stabilizes, methane is introduced at 10 sccm to initiate the growth process. The growth time varies from 30 minutes to 3 hours, depending on the desired coverage of graphene. After the growth, the upper portion of the furnace is opened to quickly cool down the sample.

2. Graphene transfer onto various substrate

The graphene can be bubble transferred onto other substrates such as a SiO2 substrate (Figure S4), where optical microscope image, scanning electron microscope (SEM) image, or Raman spectrometry of the graphene layer can be taken to identify the graphene properties. The acquired graphene is identified to be mostly single layer (>99%).

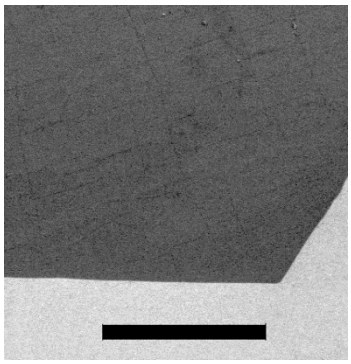

Figure S4. Graphene sample transferred onto SiO_2 substrate. Scale bar: 20 μm.

For transferring graphene onto silver or gold substrate, the metal is first annealed in hydrogen environment at 900 °C for 1 hour to remove any native oxide. The metal foils are pulled out to quickly collect graphene/PMMA layers floating on DI water. The stack is quickly loaded into a vacuum chamber (the antechamber of a glovebox) to let the water evaporate quickly. The stack is loaded into the glovebox, and baked at 180 °C for 10 min. Finally the PMMA is removed by acetone, leaving graphene covered metal substrate.

3. Raman laser parameters

The standard measurement conditions used in our experiments are described here.

Setup: Renishaw® inVia Raman Microscope.
Laser power (measured directly by a laser power meter at the objective):
4.3 mW for 785 nm solid state laser;
1.2 mW for 633 nm HeNe laser;
0.9 mW for 514 nm Ar^+ laser;
0.9 mW for 488 nm Ar^+ laser.
Integration time: 10 s.
Objective: 100x.
Laser spot size: < 1 μm.

4. Raman spectroscopy of transferred graphene on Pt

The suppression of graphene Raman signal is not limited to as-grown graphene-on-Pt samples, as measured in the transferred graphene-on-Pt samples. Graphene grown by CVD either on copper or platinum is supported by 300-nm-thick Microchem® PMMA 950 and floats on DI water bath after H_2 bubbling or copper etching. Platinum substrate is used to collect graphene samples. A very thin layer of water is introduced between graphene and the substrate by the transfer process. We first measure the Raman spectrum before water dries (Figure S5, upper curve). Distinctive G and 2D peaks from graphene can be seen together with the PMMA features. However the G and 2D peaks disappeared immediately after the water buffering layer is removed by baking the sample at 180 ˚C for 5 min (Figure S5, lower curve). It is also noted that samples prepared by room temperature drying does not have quenched graphene Raman signal, especially for graphene samples acquired from CVD growth on copper. This is probably due to the reflow of PMMA above its glass transition temperature eliminates any gaps between graphene and Pt.

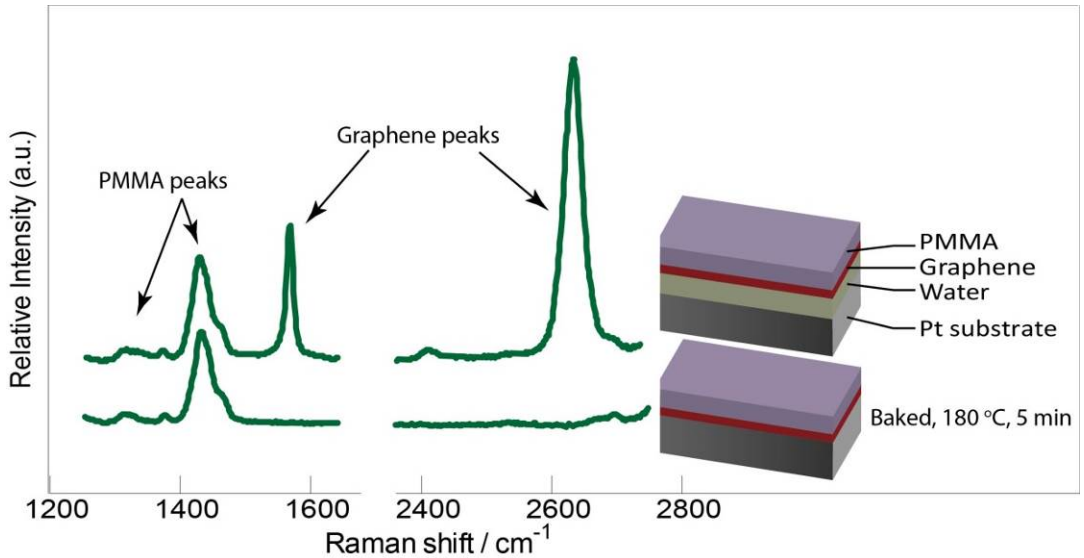

Figure S5. The quenching of Raman signal for transferred graphene-on-Pt samples.

5. Raman measured with different photon energy

Figure S6 shows the Raman spectrum measured at the same location of a graphene-on-Pt sample with different laser wavelengths (633 nm laser usually generates weaker Raman signal due to larger screening effect at this wavelength). While the G peak appears to be consistent at different locations, 2D peak can be highly dependent on photon energies. For example, at some locations, 2D peak shows up at one wavelength but is totally not detectable at another. At some other locations, the situation could be reversed. In the particular location shown in Figure S6, 2D peak is not detectable by 633 nm laser while show up when measured by 514 nm or 488 nm laser. The explanation of this effect can be found in the main text.

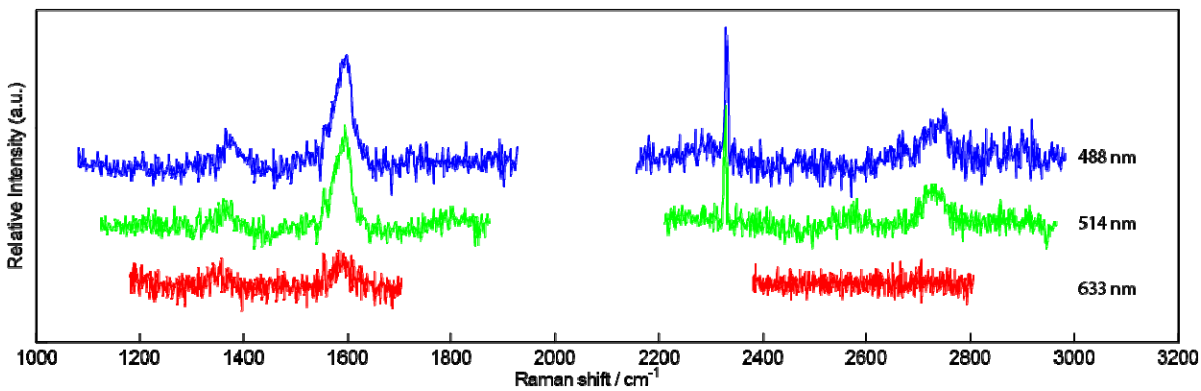

Figure S6. Raman spectrum of graphene on Pt measured at the same spot of a sample with different laser wavelengths. The integration time is 500s.

Figure S7 shows the Raman spectrum for a specific graphene-platinum superstructure: R30 2 × 2 [3]. The modified graphene band structure can be found in the main text.

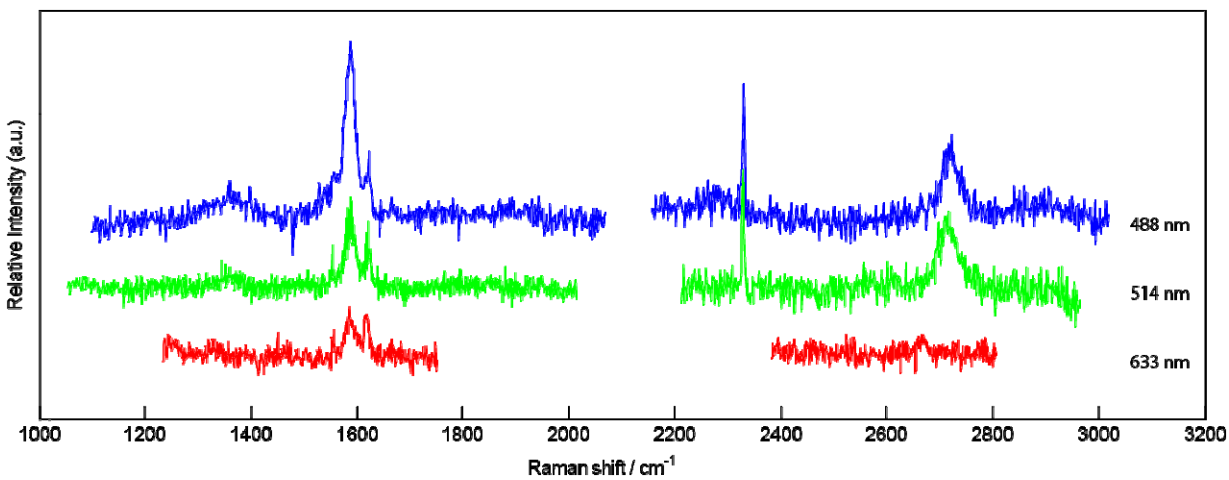

Figure S7. Raman spectrum of graphene on Pt (111) with R30 2x2 supercell structure. The integration time is 500s.

Figure S8 shows the Raman spectrum for a specific graphene-Iridium superstructure: R0 [4]. Due to stronger graphene-substrate interaction, graphene appears on Ir(111) surface mostly as R0 or R30 superstructure. In case of R0 shown here, 2D peak is not detectable and G peak is strongly altered. In case of R30 supercell, Raman spectrum is easier to detect and does not deviate much from free-standing graphene [4].

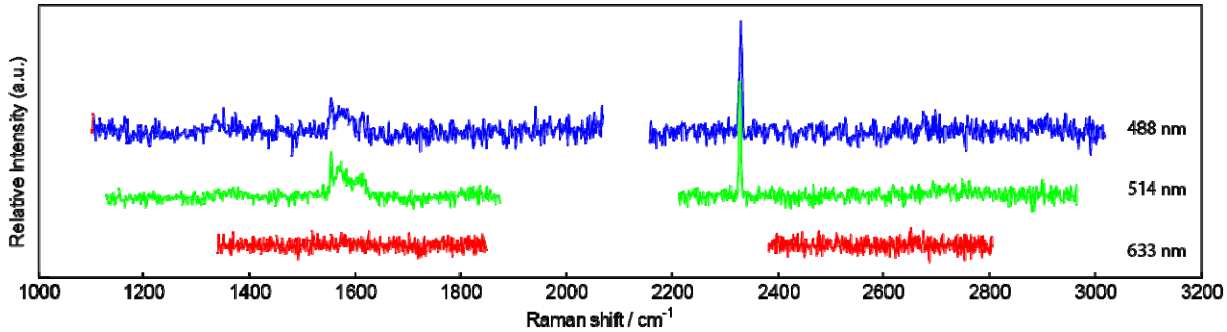

Figure S8. Raman spectrum of graphene on Ir (111) with R0 supercell structure. The integration time is 500s.

6. SEM pictures of graphene on Pt foil sample used for Raman mapping

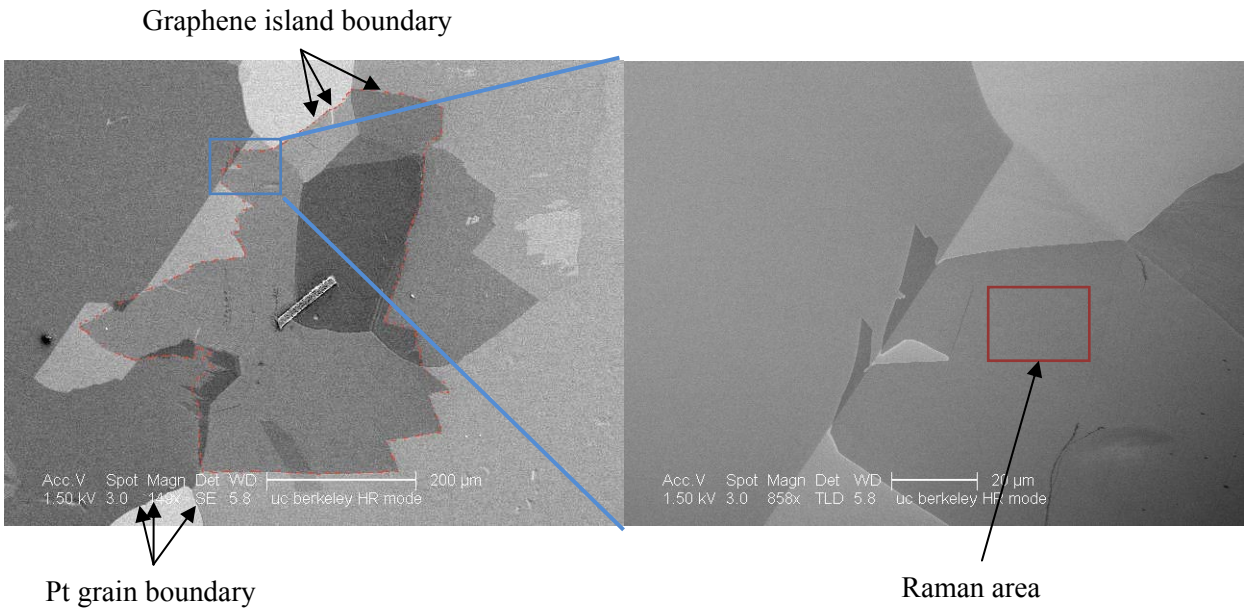

Figure S9. The SEM pictures of the sample of graphene on Pt foil used for Raman mapping (Fig.4 inset, main text). The graphene island boundary in the left panel is delineated with red dotted lines.

7. Determining the superstructure of graphene on Pt (111)

The crystalline direction of Pt (111) surface is determined by low energy electron diffraction (LEED) as shown in Figure S10. Since the LEED has a beam size of ~ 1 mm, we are not able to directly determine the orientation of the graphene island. Alternatively, the crystalline orientation of the graphene island is determined from the straight edges of the graphene island, as shown in a SEM picture Figure S11. Previous studies found that the edge of the graphene island can either be zigzag or armchair [1], so our measurements in LEED and SEM leaves us two possible graphene-Pt angles: 0.7°±1.3° or 30.7°±1.3°. The first case corresponds to several possible superstructures, named phase λ, μ,ν,ξ, and o [3]. These supercells are large-sized (e.g. ξ phase is 8 × 8 graphene supercell) and difficult to grow into large island [5]. During the cooling process, all these phases are possible to form, causing inhomogeneous Raman features across the graphene island (like the case in Fig.4, main text). Since this graphene island is among the largest, and the homogeneous Raman signal features across the island, we can eliminate the

first case (0.7°±1.3°). The second case, 30.7°±1.3°, only corresponds to one superstructure: α phase [3]. This explains why consistent Raman signal is observed across the whole graphene island. This phase is also routinely observed in literatures and have high graphene growth rate [5]. We therefore conclude that this graphene island formed 2 × 2 supercell structure with Pt (111) substrate.

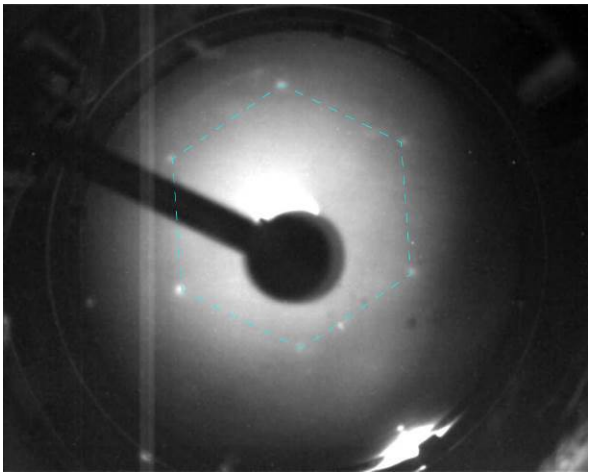

Figure S10. LEED pattern of the Pt(111) single crystal.

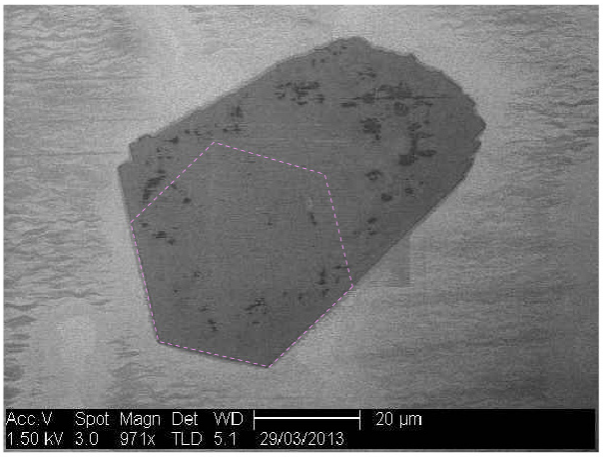

Figure S11. SEM picture of the graphene island on Pt (111) used for Raman measurement. The dirt on the island is imprinted intentionally by a piece of polymer tape so that later the island can be located under optical microscope for Raman measurement.

8. Influence of hybridization on Raman 2D and G signal

Figures S12 and S13 show computed position and width of Raman 2D signal in graphene hybridized with a single metallic d-orbital per graphene unit cell. We find similar trends as in the case of Raman 2D intensity shown in the main text in Figure 3. The incoming photon energy in this calculation is 1.96 eV, and vertical distance from the metallic d-orbital to the graphene layer is kept constant at 3.3Å. Hybridization parameters are taken from the full density functional theory calculation.

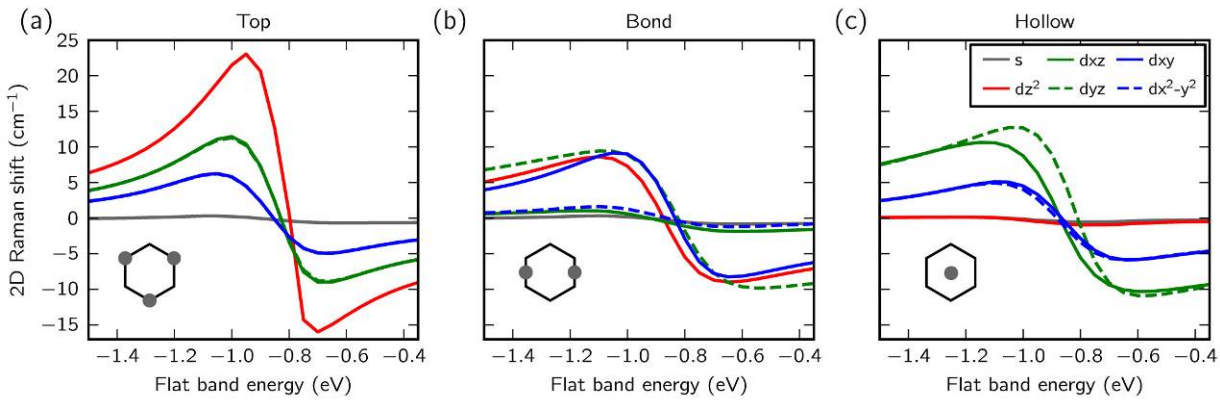

Figure S12. Computed shift of the graphene Raman 2D signal (with respect to the clean graphene) upon hybridization with a metallic flat band (assuming only one metallic orbital per graphene unit cell). Conventions are the same as in Fig. 3 in the main text.

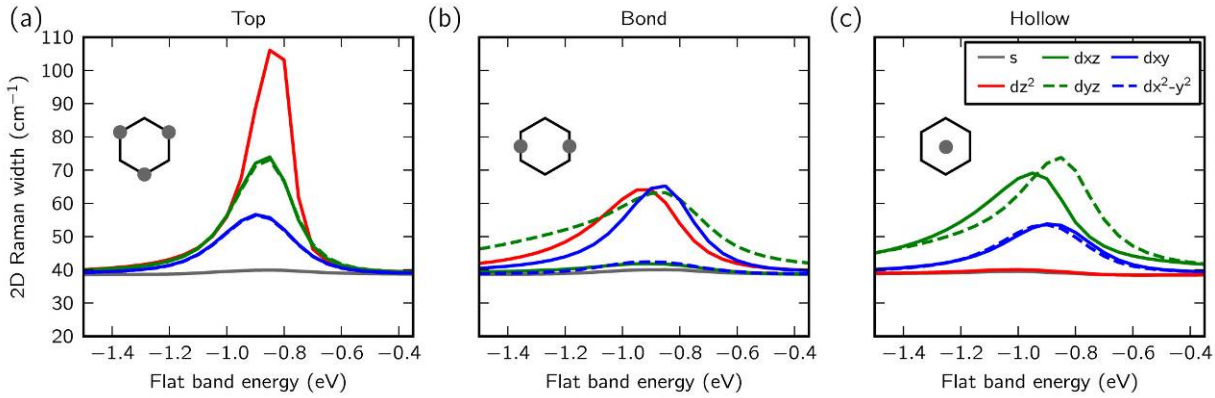

Figure S13. Computed width (FWHM) of graphene Raman 2D signal upon hybridization with a metallic flat band (assuming only one metallic orbital per graphene unit cell). Conventions are the same as in Fig. 3 in the main text.

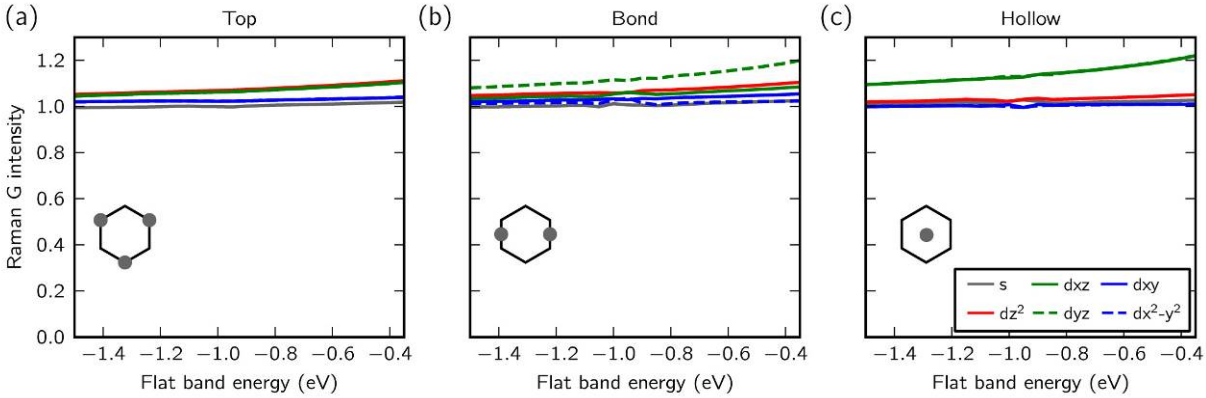

Figure S14. Slight increase in graphene Raman G signal intensity upon hybridization with a metallic flat band (assuming only one metallic orbital per graphene unit cell). Conventions are the same as in Fig. 3 in the main text.

Figure S15 shows computed Raman profiles of graphene hybridized with a single metallic dz2 orbital per graphene unit cell. We find strong modifications of the Raman signal if dz2 orbital is placed either in *top* or *bond* sites, while it shows nearly no effect if placed in the *hollow* site. Same effect is also shown in Fig. 3 in the main text, and in Fig. S12 and S13 in this supplement. On top of variations in intensity, width, and peak position, we also find that the peak shape is deviating from a Gaussian shape and that it shows multiple peak substructure, especially when metallic orbital is aligned with the incoming laser photon energy (lines near the middle of Fig. S15).

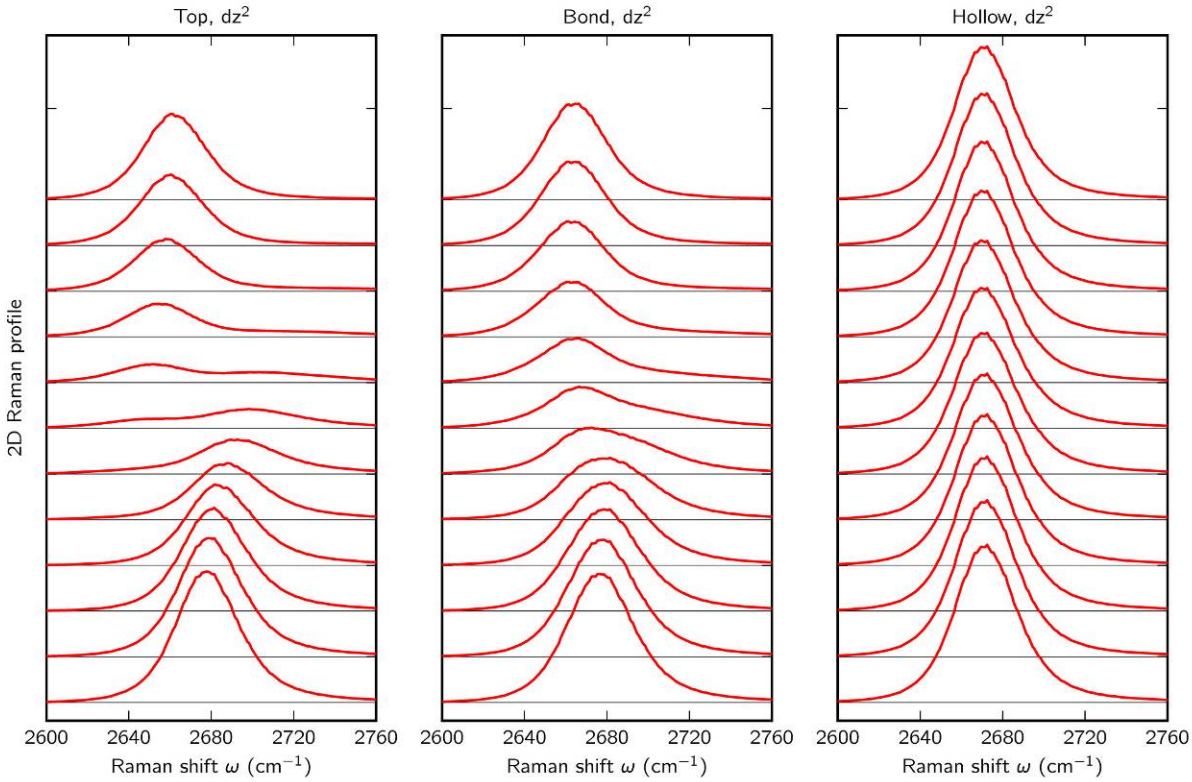

Figure S15. Calculated Raman 2D profiles of graphene upon hybridization with a metallic flat band (with only one metallic orbital per graphene unit cell). Metallic d-orbital character in each case is dz2, position of the orbital with respect to the graphene lattice is varied among three panels, and energy of the orbital with respect to the Dirac point is tuned from -1.5 eV (bottom line) to -0.4 eV (top line) in steps of 0.1 eV. Energy of the incoming laser photons is 1.96 eV.

9. Parameterization of the simplified tight-binding model

We parameterize density functional calculations of graphene on platinum and gold using a simple Slater-Koster parameterization. We first construct maximally localized Wannier functions [6] for pz orbitals in graphene and for s and d orbitals in metal (both Pt and Au). Next we fit Hamiltonian matrix elements in the Wannier function basis using a Slater-Koster parameterization [7]. Best fit parameters are given in the table below. In the fit we assume simple decay of the matrix elements of the form $\sim exp[-(r-3.3A)^3]$, so that it equals exactly 1 whenever distance between the orbitals (r) equals distance between graphene and metal substrate (z=3.3 A).

	pz - s	pz-d (sigma orientation)	pz-d (pi orientation)
Platinum	-0.22 eV	-0.24 eV	-0.19 eV
Gold	-0.24 eV	-0.24 eV	-0.16 eV

10. Electronic structure of graphene on gold substrate

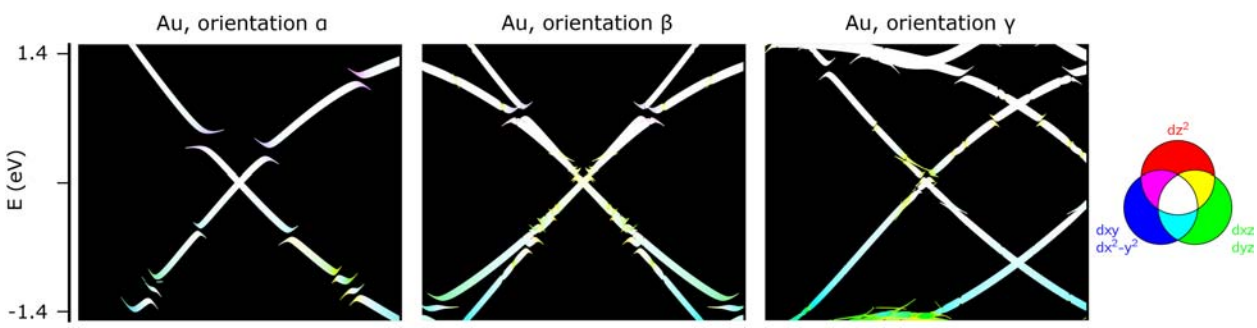

Figure S16. The electron band structure of graphene on gold substrate. There is negligible influence of gold substrate on the graphene states near the Dirac point. Conventions used here are the same as in the Fig. 2 in the main text.

REFERENCES

[1] L. Gao, W. Ren, H. Xu, L. Jin, Z. Wang, T. Ma, L.-P. Ma, Z. Zhang, Q. Fu, L.-M. Peng, X. Bao, and H.-M. Cheng, Nature Communications **3**, 699 (2012).

[2] J. Ping and M. S. Fuhrer, ArXiv 1304.5123 (2013).

[3] P. Merino, M. Svec, and A. Pinardi, ACS Nano **5**, 5627 (2011).

[4] E. Starodub, A. Bostwick, L. Moreschini, S. Nie, F. El Gabaly, K. F. McCarty, and E. Rotenberg, Physical Review B **83**, 125428 (2011).

[5] P. Sutter, J. T. Sadowski, and E. Sutter, Physical Review B **80**, 1 (2009).

[6] N. Marzari and D. Vanderbilt, Physical Review B **56**, 12847 (1997).

[7] J. Slater and G. Koster, Physical Review **94**, 1498 (1954).